Numerical Solution of Advection-Diffusion Equations for Radial Flow

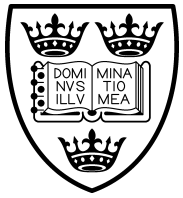

Tamora James

Wadham College

University of Oxford

Submitted in partial fulfillment of the degree of

Master of Science

in Mathematical Modelling and Scientific Computing

Summer 2002

Acknowledgements

I would like to thank my supervisors, Dr Ian Sobey of Oxford University Computing Laboratory and Dr John Sherwood of Schlumberger Cambridge Research, for their patience and assistance. Thanks also to Professor C.M. Elliott, University of Sussex, for technical and moral support.

Contents

0.5pt0pt

Chapter 1

Introduction

Sherwood [12] proposes a model for the squeeze flow of cement and other paste suspensions between two approaching parallel circular plates. Such tests provide information about the behaviour of these materials under the high stresses to which they may be subjected in the field, typically by measuring the amount of force required to push the plates together. However, in general the materials used are non-Newtonian fluids, meaning that the relationship between stress and strain for the materials is non-linear [3], so it is difficult to determine what is happening to the paste from such experimental data. There is industrial interest in *rheology*, the study of the behaviour of these pastes, because it is desirable to avoid anomalous behaviour in the field.

The pastes are dense suspensions of solid particles in liquid phase. Observations suggest that, for some pastes, flow of liquid relative to solid is non-negligible. This suggests that a two phase analysis is more appropriate than treating the paste as a homogeneous material. The analysis of Sherwood [12], based on constant velocity squeeze flow of a plastic material with slip at the walls, distinguishes between solid and liquid volume fractions. He obtains the following governing equation for the solid volume fraction, ϕ, of the paste ((24) of [12]), which is one-dimensional, since it is independent of the coordinate normal to the plates and radial symmetry is assumed:

$$\frac{\partial}{\partial t}(h\phi) = -\frac{1}{r}\frac{\partial}{\partial r}\Big[rh\phi u_{\mathrm{rad}} + \frac{rh\kappa\phi}{\mu}\frac{\partial p}{\partial r}\Big]. \tag{1.1}$$

Here, h is the distance between the plates, κ is the permeability of the paste, μ is the viscosity of the liquid fraction and p is the pore pressure of the liquid fraction. The motion of the liquid relative to the solid fraction

is assumed to obey Darcy's law,

$$u_l = -\frac{\kappa}{\mu}\nabla p, \tag{1.2}$$

and the total velocity is obtained by adding the solid velocity u_s,

$$u_\mathrm{s} - \frac{\kappa}{\mu}\frac{\partial p}{\partial r} = u_\mathrm{rad} \equiv \frac{Ur}{h}, \tag{1.3}$$

assuming that the plates move together with velocity U. Then, using an expression for the pore pressure gradient derived from the lubrication analysis ((12) of [12]), (1.1) may be rewritten in the form of an advection-diffusion equation for $h\phi$,

$$\frac{\partial}{\partial t}(h\phi) = -\frac{1}{r}\frac{\partial}{\partial r}\Big[r^2\phi U - \frac{r\kappa\phi}{\mu}\big(2f + \frac{\mathrm{d}\psi}{\mathrm{d}\phi}\frac{\partial}{\partial r}(h\phi)\big)\Big]. \tag{1.4}$$

f represents the shear stress at the plates and ψ is the isotropic stress within the solid matrix.

This provides a motivating example for an investigation of radial flow models for advection-diffusion equations. Another example is radial Darcy flow away from or towards a well bore [2], with

$$u_\mathrm{rad} = \frac{Q}{2\pi r}, \tag{1.5}$$

where Q is the flow rate. The radial spreading of a front caused by the diffusive terms in such equations is accentuated due to the fact that the flow velocity is proportional to the radial coordinate. Numerical schemes must be constructed with care, since added numerical inaccuracies may result in a severe overall loss of information.

The aim of this report is to formulate a simple model for radial flow and to discuss strategies for the numerical solution of radial advection-diffusion equations. Numerical first order schemes produce numerical diffusion which causes the smearing of sharp fronts in the solution, even in the absence of physical diffusion (see Figure 14 of [12]). Second order schemes, whilst having greater accuracy, notoriously suffer from oscillations which can produce non-physical results near steep gradients. However, second order schemes may be modified, using the technique of *flux-limiting*, to prevent overshoots in the solution. The class of flux-limited methods has been studied in the literature for linear and general scalar one-dimensional

equations (e.g. [5], [6], [7], [13]), but does not seem to have been developed for radial flows, although the motivation to use these so-called *high resolution methods* is great. LeVeque [9] provides the following criteria which are satisfied by high resolution methods:

- second order accuracy in smooth regions of a solution;
- sharp resolution of shocks without excessive smearing;
- absence of spurious oscillations;
- consistency with a conservation law;
- satisfaction of a discrete entropy condition;
- stability bound useful for convergence results.

These conditions will be studied in the context of radial flow equations in order to develop an understanding of the application of flux-limited schemes in the solution of radial problems.

0.5pt0pt

Chapter 2

Formulation of Radial Flow Model

We wish to derive a model for radial flow which incorporates advection, caused by a flow velocity, and diffusion, due to random molecular redistribution. For the purposes of this report we consider a simplified model which does not take into account the details of the rheological properties of the test materials used in the industry. Sherwood [12] provides a detailed account of the processes to be factored into a full model.

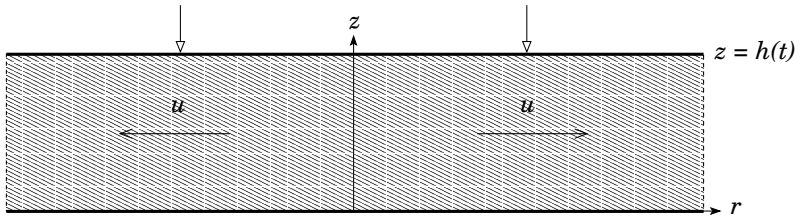

Figure 2.1: Squeeze test.

We suppose that a sample of a homogeneous test material is placed between two parallel plates which are gradually squeezed together, producing a radial flow velocity (Figure 2.1). According to Sherwood, a slip boundary condition at the plates is appropriate, since pastes are known to slip at the walls of rheometers. In Sherwood's model, allowing slip leads to a one-dimensional problem, since gradients across the gap between the plates become negligible. The free slip boundary condition is used for the simple model considered here. Sherwood also assumes that the paste completely fills the gap between the plates, with extruded paste being removed in some way at the outer edge, so that the spatial domain is fixed throughout the test. Sherwood notes the difficulty of choosing an appropriate boundary condition at the periphery. It may be necessary to

use experimental data obtained by monitoring the state of the extruded paste.

2.1 Squeeze Flow Model

The flow model is set up using mass balance arguments. Suppose the plates are at $z = 0$ and $z = h(t)$ where the distance between the plates, $h(t)$, is a given function. Assume that the squeezing motion sets up a radial velocity which is independent of the axial coordinate. This allows free slip at the plates. To determine the radial velocity, consider

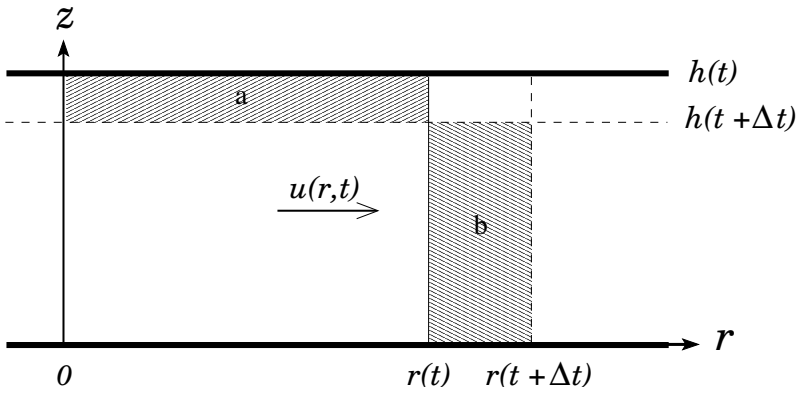

Figure 2.2: Volume balance for the flow model.

the portion of material between the origin and a radius r and balance the volume displaced by the motion of the plates with the flux of material in this section. In a small time Δt, the change in volume due to compression of the plates (area a in Figure 2.2) is approximately

$$\pi r^2(h(t) - h(t + \Delta t)), \tag{2.1}$$

while the radial flux past r (area b in Figure 2.2) is

$$2\pi r h u(r, t)\Delta t, \tag{2.2}$$

so that in the limit, as $\Delta t \to 0$,

$$u(r, t) = -\frac{1}{2}\frac{\dot{h}}{h}r. \tag{2.3}$$

Later we will examine particular cases for the distance function $h(t)$.

A physical quantity of interest to rheologists performing the squeeze test is the volume fraction of solid within the paste. To generalize this notion, suppose that we are interested in the concentration, $c = c(r, t)$, of some substance within the fluid and suppose that the fluid has constant radial diffusivity D. Balancing the mass of the substance in a control volume as above yields

$$\frac{\partial}{\partial t}(rhc) + \frac{\partial}{\partial r}(rhcu) = \frac{\partial}{\partial r}\Big(Drh\frac{\partial c}{\partial r}\Big). \tag{2.4}$$

It is convenient to define an auxiliary variable

$$s = rhc, \tag{2.5}$$

so that the equation of motion (2.4) becomes

$$\frac{\partial s}{\partial t} + \frac{\partial}{\partial r}(us) = D\frac{\partial}{\partial r}\Big(r\frac{\partial}{\partial r}\frac{s}{r}\Big). \tag{2.6}$$

The coefficient D in (2.4) and (2.6) moderates the amount of diffusion at work in the fluid and is assumed in this work to be constant, although it may be the case that D depends locally on the concentration c. Sherwood [12] gives the following constitutive relationship for the diffusivity of a bentonite suspension,

$$D = D_0 e(\phi)^{-\beta}, \tag{2.7}$$

where $e(\phi)$ is the ratio of solid to liquid fraction, known as the *void ratio*. For bentonite, the values of D_0 and β are

$$D_0 = 1.8 \times 10^{-10}\,\mathrm{m^2\,s^{-1}}, \qquad \beta = 1.92. \tag{2.8}$$

These constants may be modified to simulate the behaviour of different pastes.

We now suppose that the squeezing motion is regulated in such a way that the distance between the plates is reduced exponentially,

$$h(t) = h_o\,\exp(-2U_o t), \tag{2.9}$$

so that the velocity is time independent. Then the velocity takes the form

$$u(r) = U_o r, \tag{2.10}$$

where $U_o \equiv -\frac{1}{2}\frac{\dot{h}}{h}$ is a constant. This is equivalent to the radial velocity (1.3), where U represents half of the total plate velocity. In this case, (2.6) becomes

$$\frac{\partial s}{\partial t} + \frac{\partial}{\partial r}(U_o r s) = D\frac{\partial}{\partial r}\Big(r\frac{\partial}{\partial r}\frac{s}{r}\Big). \tag{2.11}$$

The distinction between the equation and normal advection diffusion equations is now clear, since the space variable r occurs within both spatial derivatives. When studying advection diffusion equations it is common to use the conservation form

$$\frac{\partial s}{\partial t} + \frac{\partial f}{\partial r} = 0, \tag{2.12}$$

where the flux f is usually a function of s only, $f = f(s)$. Rewriting (2.11) in the form of a conservation law,

$$\frac{\partial s}{\partial t} + \frac{\partial}{\partial r}\Big[r\Big(U_o s - D\frac{\partial}{\partial r}\frac{s}{r}\Big)\Big] = 0. \tag{2.13}$$

This equation differs from conservation equations usually studied in the literature (e.g. [7], [9]) in that the bracketed flux term depends both upon the dependent variable $s(r,t)$ and the independent variable r,

$$f \equiv f(r,s) = r\Big(U_o s - D\frac{\partial}{\partial r}\frac{s}{r}\Big). \tag{2.14}$$

The extra dependence on the spatial variable must be taken into account when constructing numerical methods for the flow. In Chapter 3, general numerical methods for the case $f \equiv f(s)$ will be outlined. Specific methods for the case $f \equiv f(r,s)$ will be developed in Chapter 4.

To complete the model we must define boundary and initial conditions for the flow. Assuming an initial concentration profile $c_o(r)$ and height h_o gives the initial condition

$$s(r,0) = r h_o c_o(r). \tag{2.15}$$

Using (2.5), at $r = 0$ we simply have $s = 0$. Choosing a condition for the outside edge of the plates is more difficult. We will assume that the radius R of the plates is large and that the initial concentration is fixed, $c = c_\infty$, outside this radius. Then, as long as the final time is not too large, we may be confident that the concentration is constant at the exterior edge of the plates throughout the test, leading to a fixed boundary condition at $r = R$.

To summarize, the model is as follows:

$$\frac{\partial s}{\partial t} + \frac{\partial}{\partial r}\Big[r\Big(U_o s - D\frac{\partial}{\partial r}\frac{s}{r}\Big)\Big] = 0, \qquad 0 \le r \le R,\ t > 0; \tag{2.16}$$

$$s(r,0) = r h_o c_o(r), \qquad 0 \le r \le R; \tag{2.17}$$

$$\left.\begin{aligned} s(0,t) &= 0, \\ s(R,t) &= Rh(t)c_\infty, \end{aligned}\right\} \qquad t > 0. \tag{2.18}$$

2.2 Analytical Solution

The governing equation may be rescaled to remove its parameters. Natural scales for r, t are R, U_o respectively. Defining dimensionless variables

$$\hat{r} = \frac{r}{R}, \quad \hat{t} = U_o t, \tag{2.19}$$

and substituting for r, t in (2.16) yields, after cancellation,

$$\frac{\partial \hat{s}}{\partial \hat{t}} + \frac{\partial}{\partial \hat{r}}\Big[\hat{r}\Big(\hat{s} - \frac{D}{U_o R^2}\frac{\partial}{\partial \hat{r}}\frac{\hat{s}}{\hat{r}}\Big)\Big] = 0, \tag{2.20}$$

where $\hat{s} = \hat{s}(\hat{r}, \hat{t})$. The initial and boundary conditions, (2.17), (2.18), become

$$\hat{s}(\hat{r},0) = R h_o \hat{r}\hat{c}_o, \quad \hat{s}(0,\hat{t}) = 0, \quad \hat{s}(1,\hat{t}) = R\hat{h}c_\infty. \tag{2.21}$$

Dropping carets, (2.20) becomes

$$\frac{\partial s}{\partial t} + \frac{\partial}{\partial r}\Big[r\Big(s - \lambda\frac{\partial}{\partial r}\frac{s}{r}\Big)\Big] = 0, \tag{2.22}$$

where λ denotes the dimensionless quantity

$$\lambda = \frac{D}{U_o R^2}. \tag{2.23}$$

This is exactly the reciprocal of the parameter $\tilde{U}$ occurring in the non-dimensionalised equation (43) of Sherwood [12] (*cf.* (1.4)),

$$\tilde{U}\frac{\partial}{\partial \tilde{t}}(\tilde{h}\phi) = -\frac{1}{\tilde{r}}\frac{\partial}{\partial \tilde{r}}\Big[\tilde{r}^2\phi\tilde{U} - 2\alpha\tilde{r}\Big(\frac{\lambda_f R_0}{h_0}\Big)\Big(\frac{1-\phi}{\phi}\Big)^{1-\beta} - \frac{\tilde{r}}{\phi^{2-\beta}(1-\phi)^\beta}\frac{\partial}{\partial \tilde{r}}(\tilde{h}\phi)\Big], \tag{2.24}$$

where $\tilde{U}$ is defined by

$$\tilde{U} = \frac{UR_0^2}{D_0 h_0}. \tag{2.25}$$

According to Sherwood, $\tilde{U}$ plays the rôle of a Péclet number, a quantity which gives a measure of the relative importance of advective and diffusive processes [10]. For $\tilde{U} = 1$, the diffusion term dominates equation (2.24), with diffusive effects decreasing as $\tilde{U}$ is increased (see Figure (21) of [12]). We can draw similar conclusions by considering the effect of varying λ. When λ is large, the most important term in (2.22) is the diffusion term. For small λ, we expect advection to be the dominant process.

Eqn. (2.22) can be rescaled by setting

$$r = \sqrt{\lambda}\rho, \tag{2.26}$$

giving a parameterless form,

$$\frac{\partial s}{\partial t} + \frac{\partial}{\partial \rho}\Big[\rho\Big(s - \frac{\partial}{\partial \rho}\frac{s}{\rho}\Big)\Big] = 0. \tag{2.27}$$

The domain becomes $0 \leq \rho \leq \lambda^{-\frac{1}{2}}$. This is a non-constant coefficient, linear equation which, in principle, can be tackled analytically. Using a Laplace transform with

$$\bar{s}(\rho, p) = \int_0^\infty \mathrm{e}^{-pt} s(\rho, t)\mathrm{d}t, \tag{2.28}$$

and initial data $s(\rho, 0) = s_0(\rho)$, the governing equation becomes an ordinary differential equation in ρ,

$$\bar{s}'' - (\rho + \rho^{-1})\bar{s}' + (\rho^{-2} - 1 - p)\bar{s} = -s_0(\rho). \tag{2.29}$$

This equation can be transformed, using the substitutions

$$z = \frac{1}{2}\rho^2, \quad \bar{s}(\rho, p) = \mathrm{e}^{z/2} w(z, p), \tag{2.30}$$

into

$$2zw'' - \Big[p + 1 + \frac{z}{2} - \frac{1}{2z}\Big]w = -\mathrm{e}^{-z/2} s_0(\sqrt{2z}). \tag{2.31}$$

The homogeneous form of this equation can be written

$$w'' + \Big[-\frac{1}{4} - \frac{p+1}{z} + \frac{1}{4z^2}\Big]w = 0. \tag{2.32}$$

This is a variant of the confluent hypergeometric equation (or Kummer's equation), and is called Whittaker's equation when in the form

$$w'' + \Big[-\frac{1}{4} + \frac{\nu}{2z} + \frac{1-4\mu^2}{4z^2} \Big] w = 0, \tag{2.33}$$

((13.1.31) of [1]), with solutions denoted $M_{\nu,\mu}(z)$ and $W_{\nu,\mu}(z)$. In the case considered here, $\nu = -(p+1)/2$ and $\mu = 0$.

In principle, a solution of the inhomogeneous equation can be found using variation of parameters. It is not likely that the resulting Laplace transform can be inverted analytically but it may be possible to apply numerical inversion (using for instance the Stehfest algorithm). It may also be possible to develop asymptotic expansions for large or small values of time (small and large p respectively) or of the parameter λ and such expansions may give results which could be used to verify numerical solutions. This approach has not been pursued in this report.

0.5pt0pt

Chapter 3

Survey of Numerical Methods

This chapter provides an overview of numerical methods and concepts which will be applied to the numerical solution of the radial flow model described in §2.1. The aim is to obtain a numerical method that provides sensible solutions with a high degree of accuracy. First we give a brief introduction to conservation laws. Then we look at upwind schemes, which yield smooth solutions but are only first order accurate. Next we consider the application of second order schemes, such as Lax-Wendroff, and find that these may produce solutions which are physically inaccurate, which is undesirable in physical applications. However, it is desirable to obtain as high an order of accuracy as possible. The notion of the total variation of a solution was introduced by Lax [8]. This measure can be used to control the generation of unwanted variation in the solution. If the total variation is non-increasing with time then this gives some convergence results and avoids the generation of spurious oscillations [9]. Since the unwanted oscillations produced by the Lax-Wendroff scheme tend to occur in regions where the gradient undergoes a rapid change, one way of reducing the oscillatory behaviour would be to introduce into the scheme a dependence on the gradient, so that the contribution from higher order terms is regulated at appropriate points. We look at the technique known as flux limiting and show how flux limited total variation non-increasing methods can be used to avoid physical inaccuracies.

3.1 Conservation Laws

A *conservation law* is a partial differential equation which can be written in the form

$$\frac{\partial s}{\partial t} + \frac{\partial f(s)}{\partial r} = 0. \tag{3.1}$$

It is useful to consider the weak formulation of conservation laws, which relaxes the differentiability requirements on the solution, thereby allowing solutions which may be physically valid despite not satisfying the PDE (3.1) across the domain. The weak formulation is derived as follows. Choosing a function $\psi(r,t)$ from the space of continuously differentiable functions on $\mathbb{R} \times \mathbb{R}^+$ which have compact support, the equation (3.1) is multiplied by ψ and then integrated with respect to r and t:

$$\int_0^\infty \int_{-\infty}^\infty [\psi s_t + \psi f(s)_r] \,\mathrm{d}r\mathrm{d}t = 0. \tag{3.2}$$

Integration by parts is used to move derivatives from s onto the smooth test function in order to obtain an equation requiring less smoothness of the solution s. From (3.2) we obtain

$$\int_0^\infty \int_{-\infty}^\infty [\psi_t s + \psi_r f(s)] \,\mathrm{d}r\mathrm{d}t = -\int_{-\infty}^\infty \psi(r,0)s(r,0) \,\mathrm{d}r. \tag{3.3}$$

A function $s(r,t)$ is a *weak solution* of (3.1) if the weak formulation (3.3) is satisfied for all test functions $\psi \in C_0^1(\mathbb{R} \times \mathbb{R}^+)$.

When constructing numerical schemes for the solution of a conservation law, using a conservative formulation ensures that the discrete solution follows the behaviour of the exact solution as closely as possible. A conservative discretization of (3.1) has the form

$$S_j^{n+1} = S_j - \frac{\Delta t}{\Delta r}\big[f^*_{j+\frac{1}{2}} - f^*_{j-\frac{1}{2}}\big], \tag{3.4}$$

where f^* is a numerical flux function based on the solution at a number of neighbouring points. We consider fluxes based on the immediate neighbouring points only,

$$f^*_{j+\frac{1}{2}} = f^*(S_j, S_{j+1}). \tag{3.5}$$

This approximates the average flux through the point $r_{j+\frac{1}{2}}$ over a time interval of length Δt [9], so that the discrete scheme resembles a mass

balance argument from which a conservation law of the form (3.1) might arise.

The scheme (3.4) is *consistent* with the original conservation law if f^* satisfies the following consistency condition, which demands that the numerical flux reduces to the actual flux in the case of constant flow,

$$f^*(s, s) = f(s). \tag{3.6}$$

Further, f^* must be Lipschitz continuous, so that the limit (3.6) is approached smoothly [9].

The following convergence result is due to Lax and Wendroff (1960).

Theorem 3.1.1 (Lax-Wendroff) *If a solution S of a consistent conservative method (3.4) converges boundedly almost everywhere to a function $s(r, t)$ when Δr, $\Delta t \to 0$ then $s(r, t)$ is a weak solution of the conservation law (3.1).*

LeVeque [9] replaces the statement "converges boundedly almost everywhere" in Theorem 3.1.1 with ℓ_1-convergence and total variation boundedness. The total variation of a function is defined in §3.4.

A weak solution is not necessarily unique and, in order to obtain the physically correct solution, an *entropy condition* of the form

$$\frac{s(r + h, t) - s(r, t)}{h} < \frac{E}{t}, \quad \forall\, h > 0, \tag{3.7}$$

should be satisfied for some constant $E > 0$. Discrete entropy conditions ensure that a consistent and convergent numerical method produces approximations which converge to the correct weak solution [9].

3.2 Upwind Methods

The technique of upwinding uses one-sided difference quotients on a discrete mesh, choosing an appropriate direction at each point. Consider, for example, the linear advection equation,

$$s_t + a s_r = 0. \tag{3.8}$$

The direction in which information propagates depends upon the sign of the constant a. It is well known that to obtain a stable upwind method, if $a > 0$ then a backwards difference quotient should be used, whereas if $a < 0$ forward differencing should be implemented.

For a general scalar equation of the form (3.1), the direction of information flow depends upon the solution itself. To derive an upwinding method for (3.1) with $f = f(s)$, we write the equation in the non-conservative form,

$$\frac{\partial s}{\partial t} + \frac{\mathrm{d}f}{\mathrm{d}s}\frac{\partial s}{\partial r} = 0, \tag{3.9}$$

and consider a linearization of the Jacobian $a(s) \equiv \frac{\mathrm{d}f}{\mathrm{d}s}$.

Consider a discrete mesh $\{r_0, r_1, \ldots, r_N\}$ with uniform spacing Δr. Let S_j, f_j denote respectively the values of the approximate solution and the flux evaluated at the jth gridpoint, i.e. $S_j^n \approx s(r_j, t_n)$ and $f_j = f(S_j)$. Using the notation

$$\Delta u_{j+\frac{1}{2}} = u_{j+1} - u_j, \tag{3.10}$$

the Jacobian may be approximated using the values of the discrete solution at neighbouring gridpoints,

$$a_{j+\frac{1}{2}} = a(S_j, S_{j+1}) = \begin{cases} \dfrac{\Delta f_{j+\frac{1}{2}}}{\Delta S_{j+\frac{1}{2}}}, & \Delta S_{j+\frac{1}{2}} \neq 0, \\ \dfrac{\mathrm{d}f}{\mathrm{d}s}(S_j), & \Delta S_{j+\frac{1}{2}} = 0. \end{cases} \tag{3.11}$$

Split $a_{j+\frac{1}{2}}$ into positive and negative contributions,

$$a^+_{j+\frac{1}{2}} = \max(0, a_{j+\frac{1}{2}}), \tag{3.12}$$

$$a^-_{j+\frac{1}{2}} = \min(0, a_{j+\frac{1}{2}}). \tag{3.13}$$

Then an upwind discretization is as follows,

$$S_j^{n+1} = S_j - \nu\{a^+_{j+\frac{1}{2}}\Delta S_{j-\frac{1}{2}} + a^-_{j+\frac{1}{2}}\Delta S_{j+\frac{1}{2}}\}, \quad \text{for } n = 0, 1, \ldots, \tag{3.14}$$

where for convenience the superscript for the nth approximation has been dropped. ν is the mesh ratio

$$\nu = \frac{\Delta t}{\Delta r}. \tag{3.15}$$

This construction ensures that the correct upwind direction is used at each point. Further, using (3.11), (3.14) can be written as

$$S_j^{n+1} = S_j - \nu[\Delta f^+_{j-\frac{1}{2}} - \Delta f^-_{j+\frac{1}{2}}], \tag{3.16}$$

where the positive and negative superscripts on $\Delta f_{j+\frac{1}{2}}$ are used to differentiate between positive and negative values as in (3.12) and (3.13). The scheme can be written in conservation form, as in §3.1,

$$S_j^{n+1} = S_j - \nu[f^U_{j+\frac{1}{2}} - f^U_{j-\frac{1}{2}}], \tag{3.17}$$

by defining $f^U_{j+\frac{1}{2}}$ using one of the following equivalent forms:

$$\begin{aligned} f^U_{j+\frac{1}{2}} &= f_{j+1} - \Delta f^+_{j+\frac{1}{2}} \\ &= f_j + \Delta f^-_{j+\frac{1}{2}} \\ &= \tfrac{1}{2}\{f_j + f_{j+1} + \Delta f^-_{j+\frac{1}{2}} - \Delta f^+_{j+\frac{1}{2}}\}. \end{aligned} \tag{3.18}$$

3.3 The Lax-Wendroff Method

The Lax-Wendroff method is obtained by modifying the inherently unstable central difference scheme. The incorporation of an extra term in the Taylor series expansion used to discretize the time derivative yields a stable scheme and improves the accuracy to second order.

Consider the Taylor series expansion

$$s_j^{n+1} = s_j^n + \Delta t \frac{\partial s}{\partial t}\Big|_j^n + \frac{\Delta t^2}{2}\frac{\partial^2 s}{\partial t^2}\Big|_j^n + O(\Delta t^3), \tag{3.19}$$

where s_j^n denotes the meshpoint value of the exact solution, $s_j^n = s(r_j, t_n)$. Using equation (3.1) we have

$$\frac{\partial s}{\partial t} = -\frac{\partial f}{\partial r} = -\frac{\mathrm{d}f}{\mathrm{d}s}\frac{\partial s}{\partial r}, \tag{3.20}$$

$$\begin{aligned} \frac{\partial^2 s}{\partial t^2} &= -\frac{\partial}{\partial r}\Big(\frac{\mathrm{d}f}{\mathrm{d}s}\frac{\partial s}{\partial t}\Big) \\ &= \frac{\partial}{\partial r}\Big(\frac{\mathrm{d}f}{\mathrm{d}s}\frac{\partial f}{\partial r}\Big). \end{aligned} \tag{3.21}$$

Then, using (3.20) and (3.21) to replace the time derivatives in (3.19) yields the approximation

$$s_j^{n+1} \approx s_j^n - \Delta t \frac{\partial f}{\partial r}\Big|_j^n + \frac{\Delta t^2}{2}\frac{\partial}{\partial r}\Big(\frac{\mathrm{d}f}{\mathrm{d}s}\frac{\partial f}{\partial r}\Big)\Big|_j^n, \tag{3.22}$$

so taking central difference approximations to the derivatives[1], and approximating the Jacobian as in (3.11), gives

$$S_j^{n+1} = S_j - \tfrac{1}{2}\nu(f_{j+1} - f_{j-1}) + \tfrac{1}{2}\nu^2[a_{j+\frac{1}{2}}\Delta f_{j+\frac{1}{2}} - a_{j-\frac{1}{2}}\Delta f_{j-\frac{1}{2}}]. \quad (3.23)$$

This may be written in conservation form (3.4) by defining a numerical flux

$$f_{j+\frac{1}{2}}^{LW} = \tfrac{1}{2}(f_j + f_{j+1}) - \tfrac{1}{2}\nu a_{j+\frac{1}{2}}\Delta f_{j+\frac{1}{2}}. \quad (3.24)$$

Writing $f_{j+\frac{1}{2}} = \frac{1}{2}(f_j + f_{j+1})$, and using the definition (3.11), this flux may be written alternatively as

$$f_{j+\frac{1}{2}}^{LW} = f_{j+\frac{1}{2}} - \tfrac{1}{2}\nu a_{j+\frac{1}{2}}^2\Delta S_{j+\frac{1}{2}}. \quad (3.25)$$

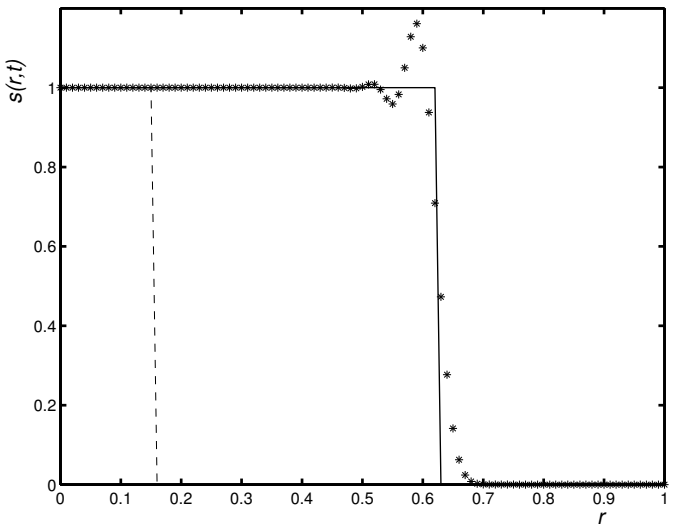

Figure 3.1: Generation of oscillations around sharp discontinuity using Lax-Wendroff scheme.

Figure 3.1 shows the result of solving the linear advection equation (3.8) using Lax-Wendroff for an initial step function. Hirsch [7] describes the analysis by Lax and Wendroff of the oscillatory behaviour generated by their scheme for solutions containing strongly varying gradients. They

[1]The related second order Warming-Beam scheme is also derived from (3.22) by using one-sided differences to second order of accuracy (see [9]).

show that the oscillations are produced by the magnification of a pointwise sign change in the local error.

In the next section, the Lax-Wendroff flux (3.25) forms the basis of a modified scheme in which numerical dispersion is limited.

3.4 TVD and Flux Limited Methods

The *total variation* of a function $u(x)$ is defined as

$$\mathrm{TV}(u(x)) = \sup \sum_k |u(x_{k+1}) - u(x_k)|, \tag{3.26}$$

where the supremum is taken over all partitions of the real line.

The following conditions are required for the convergence of a conservative finite difference scheme (3.4) to a weak solution of the corresponding conservation law (3.1) (see Harten [6]):

- uniform boundedness of the total variation of the numerical solution,
- consistency of the numerical scheme with a suitable entropy condition,
- uniqueness of the entropy satisfying weak solution.

Harten notes that it is possible to enforce the first two conditions by adding artificial viscosity terms to the finite difference scheme. These damp oscillations and simulate the selection of the vanishing viscosity weak solution (LeVeque [9]). However, numerical viscosity produces an excess of dissipation: the low resolution of first order schemes is due to the presence of a viscosity term in the truncation error (Hirsch [7]). So we expect that, as well as damping high frequency oscillations, the addition of extra dissipative terms will cause strong gradients to be smoothed out. To avoid this loss of resolution, it is necessary to ensure that additional dissipative terms act locally around sharp gradients and have a negligible effect elsewhere.

Consider the initial value problem consisting of the general scalar equation (3.1) together with initial data of bounded total variation. A weak solution of this problem satisfies the following *monotonicity properties*:

i. No new local extrema are created;

ii. The value of a local minimum is non-decreasing, and that of a local maximum is non-increasing.

Hence, the total variation with respect to the spatial variable of a weak solution is non-increasing in time,

$$\mathrm{TV}(s(r,t_2)) \leq \mathrm{TV}(s(r,t_1)) \qquad \forall\, t_2 \geq t_1. \tag{3.27}$$

We aim to construct finite difference schemes which satisfy a discrete version of the bound (3.27). This will ensure that spurious oscillations are not produced, and may also be useful for convergence results ([9]).

A numerical scheme $S^{n+1} = \mathcal{F}(S^n)$ is said to be *total variation diminishing* (TVD) if

$$\mathrm{TV}(S^{n+1}) \leq \mathrm{TV}(S^n), \qquad n = 0, 1, \ldots, \tag{3.28}$$

where

$$\mathrm{TV}(U) = \sum_{j=-\infty}^{\infty} |\Delta U_{j+\frac{1}{2}}| \tag{3.29}$$

discretizes (3.26). The TVD property is desirable because it means that spurious oscillations cannot appear in the approximate solution, as stated by the following theorem ([6]):

Theorem 3.4.1 (Harten) *A TVD scheme is monotonicity preserving.*

Monotonicity preserving means that a monotone profile is maintained when the numerical scheme is applied. It turns out that linear monotonicity preserving schemes are also *monotone*, which means that for two discrete solutions S, T,

$$S_j^n \geq T_j^n \;\; \forall j \quad \Rightarrow \quad S_j^{n+1} \geq T_j^{n+1} \;\; \forall j. \tag{3.30}$$

Since monotone schemes are at most first order accurate ([7], [9]) this means that first order accuracy is the best we can hope for from linear TVD schemes. However, non-linear schemes may be monotonicity preserving and TVD yet have second order accuracy ([6], [7]). Before considering second order TVD methods we present Harten's criteria for a numerical scheme to be TVD.

Consider a general numerical scheme written in increment form as

$$S_j^{n+1} = S_j^n - C_{j-\frac{1}{2}} \Delta S_{j-\frac{1}{2}} + D_{j+\frac{1}{2}} \Delta S_{j+\frac{1}{2}}. \tag{3.31}$$

The coefficients $C_{j-\frac{1}{2}}$, $D_{j+\frac{1}{2}}$ are functions of S^n and in general the choice of these coefficients is not unique. The following lemma (Harten [6]) gives conditions for the scheme (3.31) to be TVD.

Lemma 3.4.1 (Harten) *If C, D satisfy*

$$0 \leq C_{j+\frac{1}{2}}, \quad 0 \leq D_{j+\frac{1}{2}}, \quad 0 \leq C_{j+\frac{1}{2}} + D_{j+\frac{1}{2}} \leq 1, \tag{3.32}$$

then the scheme (3.31) is TVD.

It can be shown, by comparison with the Lax-Wendroff flux, that any three point TVD scheme is only first order accurate ([6], [7]), so to obtain a scheme with second order accuracy, more that three points must be included. As noted above, linear TVD schemes are also only first order accurate, so the extra points must be added in a non-linear way.

3.4.1 Flux-limited scheme for $s_t + as_r = 0$

To demonstrate the construction of flux limited schemes we return to the linear advection equation (3.8), with $a = 1$,

$$s_t + s_r = 0.$$

The Lax-Wendroff scheme for this equation is

$$S_j^{n+1} = S_j - \nu \Delta S_{j-\frac{1}{2}} - \tfrac{1}{2}\nu(1-\nu)[\Delta S_{j+\frac{1}{2}} - \Delta S_{j-\frac{1}{2}}] \tag{3.33}$$

This may be considered as a first order upwind scheme plus a corrective term. In terms of fluxes, the numerical flux for the Lax-Wendroff scheme is like the upwind flux with an additional term ([13])

$$f_{j+\frac{1}{2}}^{LW} = S_j + \tfrac{1}{2}(1-\nu)\Delta S_{j+\frac{1}{2}}. \tag{3.34}$$

It is clear from Figure 3.1 (p. 16) that the scheme is not TVD. Sweby suggests that the additional flux term in (3.34) should be limited by some function Φ_j which depends locally upon the solution, so that the resulting scheme

$$S_j^{n+1} = S_j - \nu \Delta S_{j-\frac{1}{2}} - \tfrac{1}{2}\nu(1-\nu)[\Phi_j \Delta S_{j+\frac{1}{2}} - \Phi_{j-1}\Delta S_{j-\frac{1}{2}}] \tag{3.35}$$

has the desired behaviour. The scheme (3.35) can be written in increment form,

$$S_j^{n+1} = S_j - \Big(\nu + \tfrac{1}{2}\nu(1-\nu)\Big[\Phi_j \frac{\Delta S_{j+\frac{1}{2}}}{\Delta S_{j-\frac{1}{2}}} - \Phi_{j-1}\Big]\Big)\Delta S_{j-\frac{1}{2}}. \tag{3.36}$$

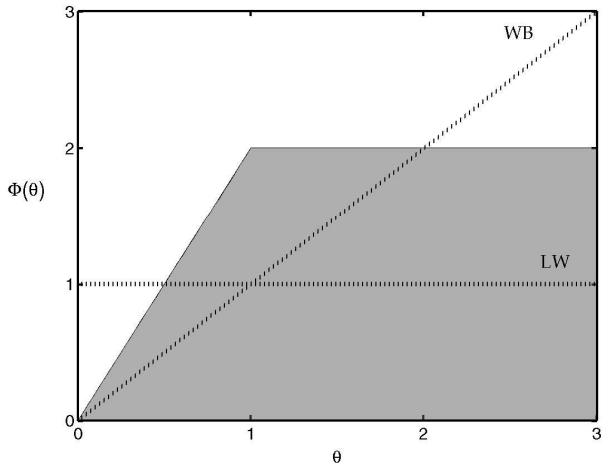

Figure 3.2: TVD region.

Now, an appropriate variable for the limiter function Φ is the ratio of consecutive gradients

$$\theta_j = \frac{\Delta S_{j-\frac{1}{2}}}{\Delta S_{j+\frac{1}{2}}}. \tag{3.37}$$

Together with (3.36), this yields the expressions for the coefficients in Harten's lemma:

$$C_{j-\frac{1}{2}} = \nu + \tfrac{1}{2}\nu(1-\nu)\Big[\frac{\Phi_j}{\theta_j} - \Phi_{j-1}\Big], \quad D_{j+\frac{1}{2}} = 0. \tag{3.38}$$

Using Lemma 3.4.1, sufficient conditions for the scheme to be TVD ([13]) are

$$\nu \leq 1 \ \text{ and } \ \Big|\frac{\Phi_j}{\theta_j} - \Phi_{j-1}\Big| \leq 2.$$

Additional requirements on Φ are non-negativity, $\Phi \geq 0$, to preserve the sign of the additional flux term, and $\Phi = 0$ for $\theta \leq 0$, since $\theta < 0$ near extreme values. Using a higher order method at these points accentuates the value of the solution and will generally cause the total variation of the solution to increase ([9]), so it is necessary to revert to the first order scheme.

Combining the above requirements gives the TVD restriction

$$0 \leq \Big(\frac{\Phi(\theta)}{\theta}, \Phi(\theta)\Big) \leq 2. \tag{3.39}$$

This is the shaded region in Figure 3.2. Note that setting $\Phi \equiv 1$ in (3.35) gives the Lax-Wendroff method. Similarly, $\Phi(\theta) = \theta$ gives the second order upwind Warming-Beam method. As shown in Figure 3.2, neither scheme lies uniformly within the TVD region, as expected considering the generation of spurious oscillations by these schemes near strongly varying gradients ([5]). Second order accuracy is obtained by demanding that Φ passes smoothly though $\Phi(1) = 1$. Sweby [13] found that to ensure that the flux-limited scheme is not overly compressive Φ should be a convex combination of the Lax-Wendroff and Warming-Beam limiters, $\Phi = 1$ and $\Phi = \theta$, as well as lying within the general TVD region. This yields the reduced second order TVD region shown in Figure 3.3.

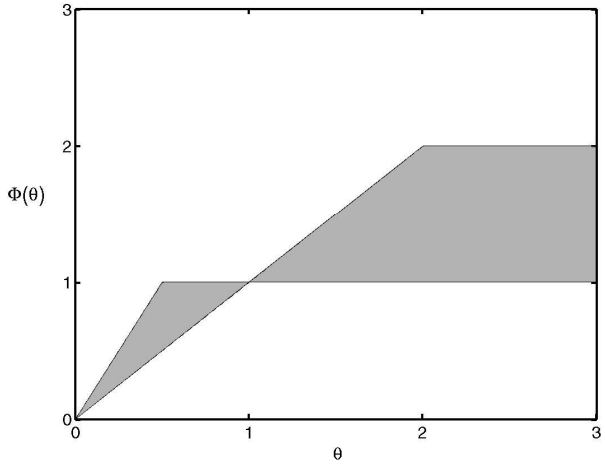

Figure 3.3: Second order TVD region.

A number of limiter functions have been developed. The simplest are the *minmod* limiter,

$$\Phi(\theta) = \min(\theta, 1), \tag{3.40}$$

and the *"superbee"* limiter, developed by Roe,

$$\Phi(\theta) = \max(0, \min(1, 2\theta), min(0, 2)). \tag{3.41}$$

These form the lower and upper boundaries respectively of the second order TVD region in Figure 3.3.

In Figure 3.4, solutions for the linear advection equation (3.8) obtained using the limiters (3.40) and (3.41) are compared with Lax-Wendroff solutions. Two sets of initial data, an exponential curve and a step function,

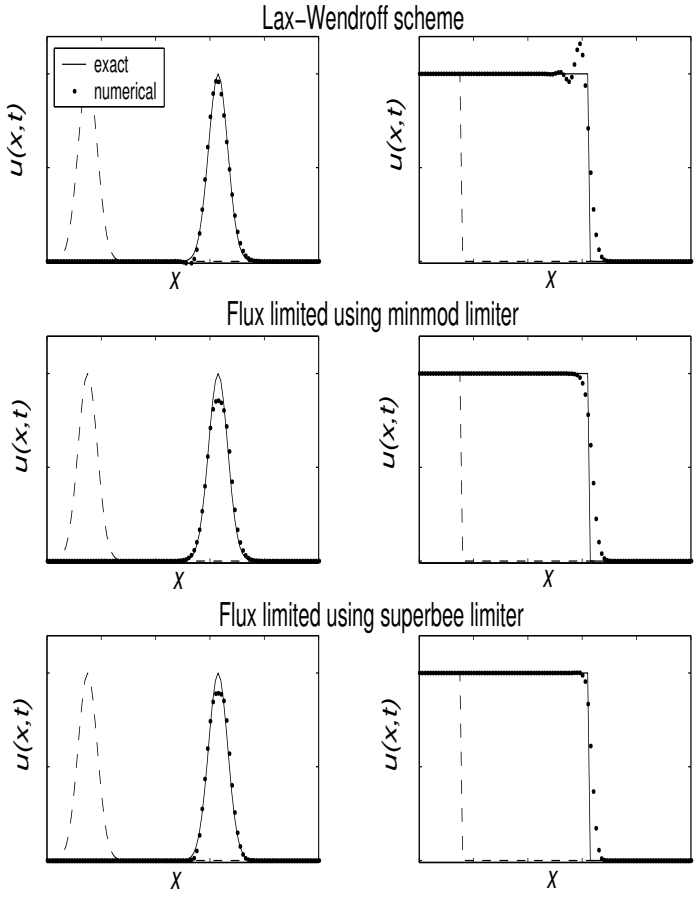

Figure 3.4: Comparison of numerical schemes for the linear advection equation.

were used. In the case of the step function, the oscillations behind the advected front that occur in the Lax-Wendroff solution are clearly eliminated in the flux-limited solutions. The Lax-Wendroff solution for the exponential data exhibits some oscillations at the base which are improved in the flux limited solution, but note the severe reduction of the maximum point of the curve. As noted earlier, loss of accuracy at extreme points is an inevitable consequence of using flux-limited schemes. The results for the superbee limiter are better than those for the minmod limiter, both in terms of accuracy at the maximum point in the case of the exponential data and of resolution of the front in the case of the step function.

3.4.2 General flux-limited schemes

Hirsch [7] describes the construction of flux limited schemes for general scalar equations of the form (3.1). The key point is a redefinition of the slope ratios (3.37). The numerical flux for the schemes comprises a first order flux supplemented with limited higher order flux terms which improve the resolution. According to Sweby, the underlying first order scheme should satisfy an entropy inequality ((2.7) of [13]),

$$\mathrm{sgn}(S_{j+1} - S_j)[f^*_{j+\frac{1}{2}} - f(s)] \leq 0, \quad \forall\, s \in (S_j, S_{j+1}), \tag{3.42}$$

to ensure convergence to the correct physical solution. Monotone schemes are known to belong to the class of entropying satisfying schemes, which are at most first order [13].

Letting f^* denote a first order monotone flux, a flux-limited second order upwind scheme is as follows (Hirsch [7])

$$\begin{aligned} S_j^{n+1} \;=\; & S_j^n - \nu\Delta_-\big[f^*_{j+\frac{1}{2}} + \tfrac{1}{2}\Phi(\theta^+_{j-\frac{1}{2}})(f_j - f^*_{j-\frac{1}{2}}) \\ & + \tfrac{1}{2}\Phi(\theta^-_{j+\frac{3}{2}})(f_{j+1} - f^*_{j+\frac{3}{2}})\big], \end{aligned} \tag{3.43}$$

where Δ_- denotes the backwards difference operator. The flux difference ratios $\theta^\pm$ are defined by

$$\theta^+_{j+\frac{1}{2}} = \frac{f_{j+2} - f^*_{j+\frac{3}{2}}}{f_{j+1} - f^*_{j+\frac{1}{2}}}, \qquad \theta^-_{j+\frac{1}{2}} = \frac{f_{j-1} - f^*_{j-\frac{1}{2}}}{f_j - f^*_{j+\frac{1}{2}}}. \tag{3.44}$$

Using these definitions, (3.43) may be rewritten as

$$\begin{aligned} S_j^{n+1} = S_j^n - \nu\Delta_-\big[& f^*_{j+\frac{1}{2}} + \\ & \tfrac{1}{2}\Phi(\theta^+_{j-\frac{1}{2}})(f_j - f^*_{j-\frac{1}{2}}) + \frac{1}{2}\frac{\Phi(\theta^-_{j+\frac{3}{2}})}{\theta^-_{j+\frac{3}{2}}}(f_j - f^*_{j+\frac{1}{2}})\big]. \end{aligned} \tag{3.45}$$

To determine whether the scheme is TVD using Lemma 3.4.1, (3.45) must be written in the incremental form (3.31). Expanding the difference op-

erator Δ_-,

$$\begin{aligned} S_j^{n+1} &= S_j^n - \nu\Big[(f^*_{j+\frac{1}{2}} - f^*_{j-\frac{1}{2}}) + \tfrac{1}{2}\Phi(\theta^+_{j-\frac{1}{2}})(f_j - f^*_{j-\frac{1}{2}}) \\ &\quad + \frac{1}{2}\frac{\Phi(\theta^-_{j+\frac{3}{2}})}{\theta^-_{j+\frac{3}{2}}}(f_j - f^*_{j+\frac{1}{2}}) - \tfrac{1}{2}\Phi(\theta^+_{j-\frac{3}{2}})(f_{j-1} - f^*_{j-\frac{3}{2}}) \\ &\quad - \frac{1}{2}\frac{\Phi(\theta^-_{j+\frac{1}{2}})}{\theta^-_{j+\frac{1}{2}}}(f_{j-1} - f^*_{j-\frac{1}{2}})\Big]. \end{aligned} \tag{3.46}$$

The flux ratios (3.44) are used to replace $(f_{j-1} - f^*_{j-\frac{3}{2}})$ and $(f_{j-1} - f^*_{j-\frac{1}{2}})$ in (3.46), yielding

$$\begin{aligned} S_j^{n+1} &= S_j^n - \nu\left[1 + \tfrac{1}{2}\Phi(\theta^+_{j-\frac{1}{2}}) - \frac{1}{2}\frac{\Phi(\theta^+_{j-\frac{3}{2}})}{\theta^+_{j-\frac{3}{2}}}\right](f_j - f^*_{j-\frac{1}{2}}) \\ &\quad - \nu\left[1 + \tfrac{1}{2}\Phi(\theta^-_{j+\frac{1}{2}}) - \frac{1}{2}\frac{\Phi(\theta^-_{j+\frac{3}{2}})}{\theta^-_{j+\frac{3}{2}}}\right](f^*_{j+\frac{1}{2}} - f_j). \end{aligned} \tag{3.47}$$

Recalling the definition (3.11) of the approximate Jacobian, define

$$a_{j+\frac{1}{2}} = \frac{f_{j+1} - f_j}{\Delta S_{j+\frac{1}{2}}}, \qquad \Delta S_{j+\frac{1}{2}} \neq 0. \tag{3.48}$$

Suppose that this expression is split into contributions from either side of the interface $r_{j+\frac{1}{2}}$, denoted by

$$a^+_{j+\frac{1}{2}} = \frac{f_{j+1} - f^*_{j+\frac{1}{2}}}{\Delta S_{j+\frac{1}{2}}}, \qquad a^-_{j+\frac{1}{2}} = \frac{f^*_{j+\frac{1}{2}} - f_j}{\Delta S_{j+\frac{1}{2}}}. \tag{3.49}$$

Then (3.47) can be written as

$$\begin{aligned} S_j^{n+1} &= S_j^n - \nu\left[1 + \tfrac{1}{2}\Phi(\theta^+_{j-\frac{1}{2}}) - \frac{1}{2}\frac{\Phi(\theta^+_{j-\frac{3}{2}})}{\theta^+_{j-\frac{3}{2}}}\right]a^+_{j-\frac{1}{2}}\Delta S_{j-\frac{1}{2}} \\ &\quad - \nu\left[1 + \tfrac{1}{2}\Phi(\theta^-_{j+\frac{1}{2}}) - \frac{1}{2}\frac{\Phi(\theta^-_{j+\frac{3}{2}})}{\theta^-_{j+\frac{3}{2}}}\right]a^-_{j+\frac{1}{2}}\Delta S_{j+\frac{1}{2}}. \end{aligned} \tag{3.50}$$

Comparing this with (3.31) gives the following expressions for the coefficients in Lemma 3.4.1,

$$C_{j-\frac{1}{2}} = \nu\left[1 + \tfrac{1}{2}\Phi(\theta^+_{j-\frac{1}{2}}) - \frac{1}{2}\frac{\Phi(\theta^+_{j-\frac{3}{2}})}{\theta^+_{j-\frac{3}{2}}}\right]a^+_{j-\frac{1}{2}}, \tag{3.51}$$

$$D_{j+\frac{1}{2}} = -\nu\left[1 + \tfrac{1}{2}\Phi(\theta^-_{j+\frac{1}{2}}) - \frac{1}{2}\frac{\Phi(\theta^-_{j+\frac{3}{2}})}{\theta^-_{j+\frac{3}{2}}}\right]a^-_{j+\frac{1}{2}}, \tag{3.52}$$

and applying Lemma 3.4.1 yields the TVD restrictions

$$\frac{\Phi(\theta^+_{j-\frac{3}{2}})}{\theta^+_{j-\frac{3}{2}}} - \Phi(\theta^+_{j-\frac{1}{2}}) \leq 2, \qquad \frac{\Phi(\theta^-_{j+\frac{3}{2}})}{\theta^-_{j+\frac{3}{2}}} - \Phi(\theta^-_{j+\frac{1}{2}}) \leq 2. \tag{3.53}$$

These conditions have the general form

$$\frac{\Phi(\theta_1)}{\theta_1} - \Phi(\theta_2) \leq 2 \tag{3.54}$$

for all θ_1, θ_2. Making the same additional requirements for general flux-limiters as for those considered in §3.4.1 leads to second order TVD restrictions of the same form as before (*cf.* (3.39)), so the same flux-limiter functions can be used to limit the general scalar equation [7].

0.5pt0pt

Chapter 4

Derivation of Numerical Methods for the Radial Model

In this chapter we focus on numerical schemes for the radial model (2.22),

$$\frac{\partial s}{\partial t} + \frac{\partial}{\partial r}\Big[r\Big(s - \lambda\frac{\partial}{\partial r}\frac{s}{r}\Big)\Big] = 0. \tag{4.1}$$

As noted in §2.1, the flux function in (4.1) has a spatial dependency and in developing numerical methods for the model this dependency must be dealt with correctly.

Since the model was derived using conservation arguments, it is desirable to construct conservative methods for its solution. Let

$$F^*_{j+\frac{1}{2}} = F^*(r, S^n; j) \tag{4.2}$$

denote the numerical flux approximating the flux in (2.1) at $r_{j+\frac{1}{2}}$, so that the conservation form is

$$S_j^{n+1} = S_j - \frac{\Delta t}{\Delta r}\big[F^*_{j+\frac{1}{2}} - F^*_{j-\frac{1}{2}}\big]. \tag{4.3}$$

The presence of r in the flux will cause some modifications to the methods presented in Chapter 3. These will be dealt with as they arise as far as possible. Note that applying the chain rule to (3.1) with $f = f(r, s)$ yields

$$\frac{\partial s}{\partial t} + \frac{\partial f}{\partial s}\frac{\partial s}{\partial r} + \frac{\partial f}{\partial r} = 0. \tag{4.4}$$

in which $\frac{\partial f}{\partial r}$ acts as an additional source term. It may be necessary to consider the flux

$$f(r, s) = rs, \tag{4.5}$$

and to treat the diffusion term in (2.1) separately.

4.1 Radial Lax-Wendroff

We derive a Lax-Wendroff numerical scheme to approximate the radial flow model (4.1), written as

$$\frac{\partial s}{\partial t} + \frac{\partial}{\partial r}(rs) = \frac{\partial}{\partial r}\Big(\lambda r \frac{\partial}{\partial r}\frac{s}{r}\Big). \tag{4.6}$$

The Lax-Wendroff scheme for this equation is constructed using the Taylor series expansion:

$$s(r, t+\Delta t) = s(r,t) + \Delta t s_t(r,t) + \frac{1}{2}\Delta t^2 s_{tt}(r,t) + \dots. \tag{4.7}$$

Eqn. (4.6) is used directly to replace the first time derivative in this expansion,

$$s_t = -\frac{\partial}{\partial r}(rs) + \frac{\partial}{\partial r}\Big(\lambda r \frac{\partial}{\partial r}\frac{s}{r}\Big). \tag{4.8}$$

Ignoring the diffusion term in (4.8),

$$\begin{aligned} s_{tt} &= -\frac{\partial}{\partial r}(rs_t) = \frac{\partial}{\partial r}\Big(r\frac{\partial}{\partial r}(rs)\Big) \\ &= \frac{\partial}{\partial r}\Big[r\Big(s + r\frac{\partial s}{\partial r}\Big)\Big] \\ &= \Big[\frac{\partial}{\partial r}(rs) + \frac{\partial}{\partial r}\Big(r^2\frac{\partial s}{\partial r}\Big)\Big]. \end{aligned} \tag{4.9}$$

Thus, using (4.8), (4.9) to substitute for s_t, s_{tt} in (4.7),

$$\begin{aligned} &s(r, t+\Delta t) \approx \\ &\quad s - \Delta t\frac{\partial}{\partial r}(rs) + \Delta t\frac{\partial}{\partial r}\Big(\lambda r\frac{\partial}{\partial r}\frac{s}{r}\Big) + \frac{\Delta t^2}{2}\frac{\partial}{\partial r}\Big(rs + r^2\frac{\partial s}{\partial r}\Big) \\ &= s - \Big(\Delta t - \frac{\Delta t^2}{2}\Big)\frac{\partial}{\partial r}(rs) + \frac{\Delta t^2}{2}\frac{\partial}{\partial r}\Big(r^2\frac{\partial s}{\partial r}\Big) + \Delta t\frac{\partial}{\partial r}\Big(r\frac{\partial}{\partial r}\frac{s}{r}\Big). \end{aligned} \tag{4.10}$$

The numerical scheme is now obtained by approximating the derivatives in (4.10) by central difference quotients. For convenience, let the radial grid be uniformly spaced, $r_j = j\Delta r$, $j = 0, 1, \dots, N$, and take the central difference quotients over individual grid cells. To avoid difficulties at $r = 0$ due to division by zero, the quotient in the diffusion term of (4.10) is replaced, by setting

$$\psi = \frac{s}{r} \equiv hc, \tag{4.11}$$

with reference to (2.5). Then, for grid points $j = 1, \ldots, N-1$,

$$\begin{aligned} S_j^{n+1} &= S_j^n - \Big(\frac{\Delta t}{\Delta r} - \frac{1}{2}\frac{\Delta t^2}{\Delta r}\Big)\Big(r_{j+\frac{1}{2}} S_{j+\frac{1}{2}}^n - r_{j-\frac{1}{2}} S_{j-\frac{1}{2}}^n\Big) \\ &\quad + \frac{1}{2}\frac{\Delta t^2}{\Delta r^2}\Big(r_{j+\frac{1}{2}}^2 (S_{j+1}^n - S_j^n) - r_{j-\frac{1}{2}}^2 (S_j^n - S_{j-1}^n)\Big) \\ &\quad + \lambda \frac{\Delta t}{\Delta r^2}\Big(r_{j+\frac{1}{2}}(\psi_{j+1} - \psi_j) - r_{j-\frac{1}{2}}(\psi_j - \psi_{j-1})\Big). \end{aligned} \tag{4.12}$$

Define

$$\nu = \frac{\Delta t}{\Delta r}, \quad \mu = \frac{\lambda \Delta t}{\Delta r^2}, \tag{4.13}$$

and substitute for the interface values the arithmetic mean of the values at the neighbouring gridpoints, $S_{j+\frac{1}{2}} = \frac{1}{2}(S_j + S_{j+1})$, to obtain the Lax-Wendroff scheme for the radial flow model,

$$\begin{aligned} S_j^{n+1} &= S_j - \tfrac{1}{2}\nu(1 - \tfrac{1}{2}\Delta t)\big[r_{j+\frac{1}{2}}(S_{j+1} + S_j) - r_{j-\frac{1}{2}}(S_j + S_{j-1})\big] \\ &\quad + \tfrac{1}{2}\nu^2\big[r_{j+\frac{1}{2}}^2 (S_{j+1} - S_j) - r_{j-\frac{1}{2}}^2 (S_j - S_{j-1})\big] \\ &\quad + \mu\big[r_{j+\frac{1}{2}}(\psi_{j+1} - \psi_j) - r_{j-\frac{1}{2}}(\psi_j - \psi_{j-1})\big]. \end{aligned} \tag{4.14}$$

Ignoring the diffusion term, an appropriate expression for the numerical Lax-Wendroff flux is

$$\begin{aligned} F_{j+\frac{1}{2}}^{LW} &= \tfrac{1}{2}(1 - \tfrac{1}{2}\Delta t) r_{j+\frac{1}{2}}(S_{j+1} + S_j) - \tfrac{1}{2}\nu r_{j+\frac{1}{2}}^2 (S_{j+1} - S_j) \\ &= \tfrac{1}{2} r_{j+\frac{1}{2}}(S_{j+1} + S_j) - \tfrac{1}{2}\nu r_{j+\frac{1}{2}}(r_{j+1} S_{j+1} - r_j S_j). \end{aligned} \tag{4.15}$$

Note that the dependence of the numerical flux on r has consequences for consistency. If S is constant, we obtain

$$F^*(r, S; j) = (1 - \tfrac{1}{2}\Delta t) r_{j+\frac{1}{2}} S, \tag{4.16}$$

which does not match exactly the flux $f(r_{j+\frac{1}{2}}, S) = r_{j+\frac{1}{2}} S$. The effects of this anomaly on the convergence of solutions is not known.

Results obtained using the scheme (4.14) are presented in Chapter 5. Typical Lax-Wendroff oscillations are observed when the diffusivity is set at zero. The next section considers applying the method of flux-limiters to the model equation.

4.2 Flux Limiting the Radial Model

The approach outlined in §3.4.2 is used to construct a flux-limited scheme for the radial model. We set $\lambda = 0$ in (4.1) so that the diffusive term does not appear, since diffusion smoothes out the oscillations observed in second-order methods such as Lax-Wendroff. At the core of the scheme is the first order Roe flux ([7])

$$f^R_{j+\frac{1}{2}} = \tfrac{1}{2}(f_j + f_{j+1}) - \tfrac{1}{2}\big|a_{j+\frac{1}{2}}\big|\Delta S_{j+\frac{1}{2}}, \tag{4.17}$$

where $a_{j+\frac{1}{2}}$ is defined as before by

$$a_{j+\frac{1}{2}} = \begin{cases} \dfrac{\Delta f_{j+\frac{1}{2}}}{\Delta S_{j+\frac{1}{2}}}, & \Delta S_{j+\frac{1}{2}} \neq 0, \\ \left[\dfrac{\partial f}{\partial s}\right]_j \equiv r_j, & \Delta S_{j+\frac{1}{2}} = 0. \end{cases} \tag{4.18}$$

This flux satisfies the consistency condition defined in §3.1. Indeed, if $\Delta S_{j+\frac{1}{2}} = 0$ then we have

$$f^R_{j+\frac{1}{2}} = \tfrac{1}{2}(r_j + r_{j+1})S = r_{j+\frac{1}{2}}S, \tag{4.19}$$

so the numerical flux reduces to the actual flux evaluated at the mid-point. The entropy condition (3.42) becomes [7]

$$\frac{f_j + f_{j+1} - 2f(r,s)}{\Delta S_{j+\frac{1}{2}}} \leq |a_{j+\frac{1}{2}}|, \quad \forall\, r \in (r_j, r_{j+1}),\ s(r) \in (S_j, S_{j+1}). \tag{4.20}$$

With $f(r,s) = rs$, (4.20) reduces further to

$$\min(r_j S_j, r_{j+1}S_{j+1}) - rs \leq 0, \quad \forall\, r \in (r_j, r_{j+1}),\ s(r) \in (S_j, S_{j+1}). \tag{4.21}$$

The condition is satisifed as long as the interval does not contain a local minimum for the flux. Hirsch [7] discusses methods for dealing with problems arising from the non-satisfaction of the entropy inequality.

The flux (4.17) is used to define the limiter variables, which are ratios of flux differences involving the Roe flux,

$$\theta^+_{j+\frac{1}{2}} = \frac{f_{j+2} - f^R_{j+\frac{3}{2}}}{f_{j+1} - f^R_{j+\frac{1}{2}}}, \qquad \theta^-_{j+\frac{1}{2}} = \frac{f_{j-1} - f^R_{j-\frac{1}{2}}}{f_j - f^R_{j+\frac{1}{2}}}. \tag{4.22}$$

To ensure that it is valid to form the flux ratios (4.22), it is necessary to check that the size of the flux difference in the denominator is greater than a prescribed tolerance. If this is not the case, and the numerator is also small, then θ is set at zero, while if the numerator is large, a representative large number is used for θ.

The flux-limited scheme is

$$S_j^{n+1} = S_j - \nu\big[f^{FL}_{j+\frac{1}{2}} - f^{FL}_{j-\frac{1}{2}}\big], \tag{4.23}$$

where the numerical flux f^{FL} is given by

$$f^{FL}_{j+\frac{1}{2}} = f^{R}_{j+\frac{1}{2}} + \tfrac{1}{2}\Phi\big(\theta^{+}_{j-\frac{1}{2}}\big)\big(f_j - f^{R}_{j-\frac{1}{2}}\big) - \Phi\big(\theta^{-}_{j+\frac{3}{2}}\big)\big(f_{j+1} - f^{R}_{j+\frac{3}{2}}\big). \tag{4.24}$$

MATLAB source code implementing this scheme is given in Appendix A. The code is quite complicated because the scheme requires so many auxiliary calculations, which must be carried out for a number of different, overlapping sets of grid points.

As described in §3.4, it is necessary for second order accuracy to base the discrete solution on more than three grid points. The numerical flux for the above scheme is evaluated using five different points. It should be noted that it is not possible to calculate the solution at every interior grid point using only interior values, since the second order flux (4.24) relies on quantities evaluated at the grid points and interface values over a range $(r_{j-\frac{1}{2}}, r_{j+\frac{3}{2}})$. Artificial values should be imposed at extra grid points outside the computational domain to relieve this problem. In the MATLAB implementation, at the points where the solution was not provided by the scheme (the two points interior to the boundary points) the solution was approximated by taking the average of the neighbouring values.

As noted in §3.4.2, flux-limiter functions which are valid for the linear advection equation may also be used for more general equations. In the implementation, a subfunction applies one of two choices, minmod or "superbee", of flux limiter function, according to the argument supplied. The function calculates Φ using the definitions (3.40), (3.41), and additionally imposes the condition $\Phi \geq 0$.

Results obtained from the implementation are presented in the next chapter.

0.5pt0pt

Chapter 5

Numerical Results

In Chapter 4, numerical schemes for the radial model were described. The results of the implementations of those schemes are presented here. To emulate an initial concentration of dye or some other substance near $r = 0$, a step function was used as the initial concentration profile. The codes were compared for the values $N = 100$, $\nu = 0.05$ and $\lambda = 0$ or $\lambda = 0.02$.

Figure 5.1 shows the application of the Lax-Wendroff scheme to the radial model in the absence of diffusion. Oscillations appear near the front in the solution. In Figure 5.2, the parameter λ is non-zero, and diffusion has smoothed out the region around the advecting front.

The remaining figures show results obtained using the flux-limited scheme described in §4.2. In Figure 5.3 and Figure 5.5 the minmod flux limiter was used, while the "superbee" limiter produced the results shown in Figure 5.4 and Figure 5.6. Note especially that the solutions in Figure 5.3 and Figure 5.4 are smooth, even though there is no contribution from diffusive terms. There is a slight anomaly near $r = 0$, most clearly visible in the plots of ψ against r, which is probably due to the approximation of the solution value at the first interior grid point, as discussed in §4.2. This problem is smoothed out when λ is non-zero. The effect of the diffusion term is clear from Figures 5.5 and 5.6, where $\lambda = 0.02$.

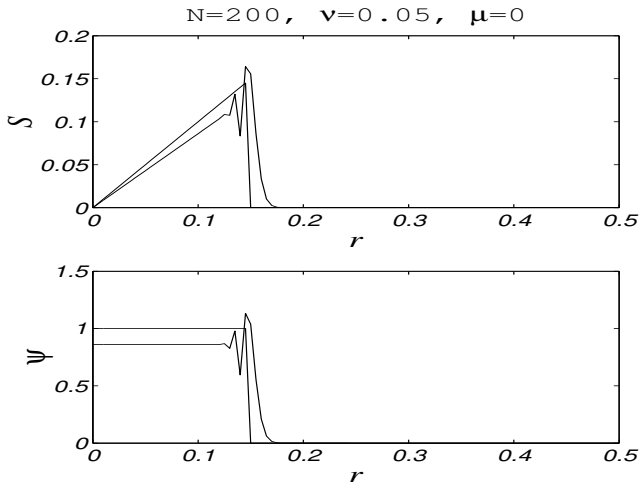

Figure 5.1: Lax Wendroff scheme, $\lambda = 0$.

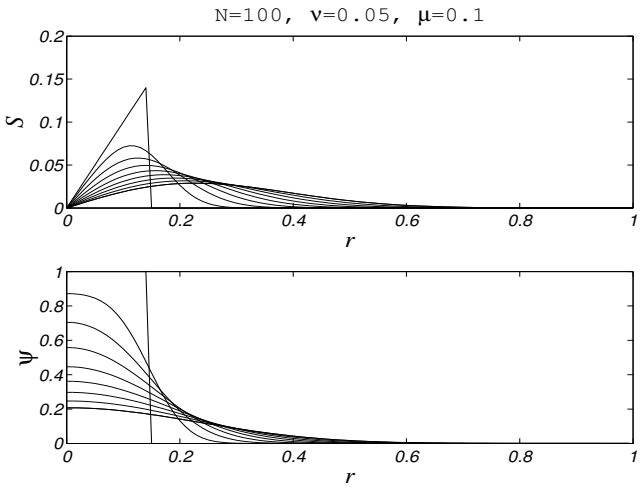

Figure 5.2: Lax Wendroff scheme, $\lambda = 0.02$.

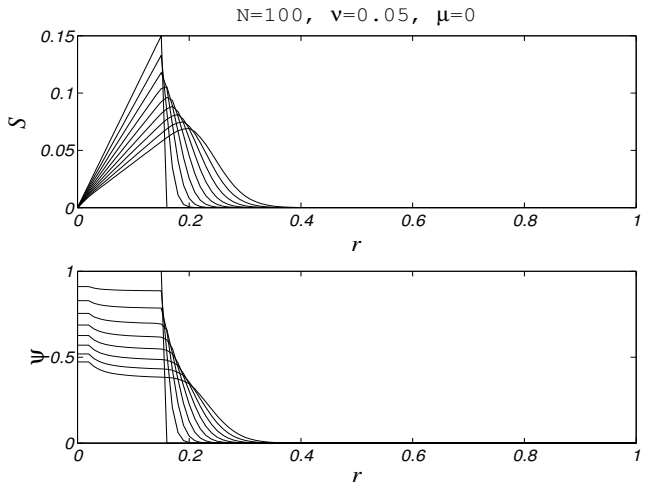

Figure 5.3: Flux-limited scheme using minmod limiter, $\lambda = 0$.

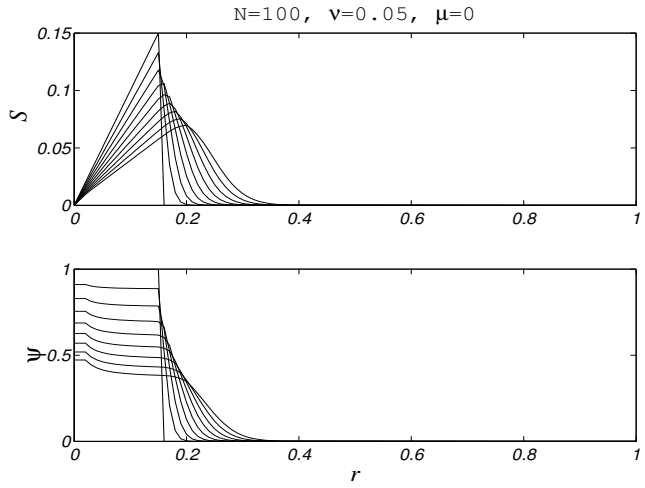

Figure 5.4: Flux-limited scheme using "superbee" limiter, $\lambda = 0$.

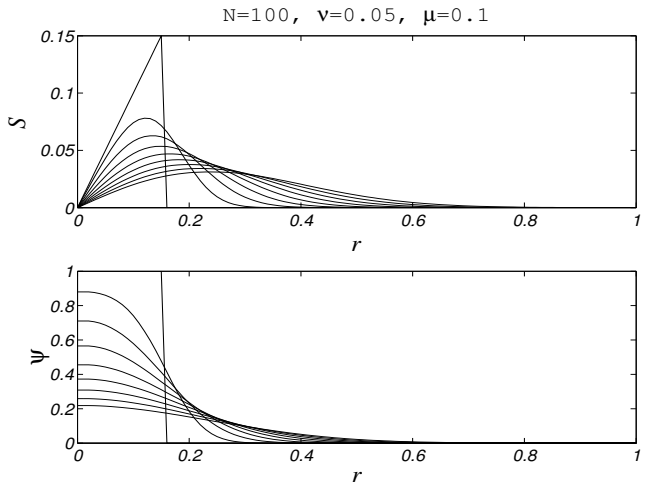

Figure 5.5: Flux-limited scheme using minmod limiter, $\lambda = 0.02$.

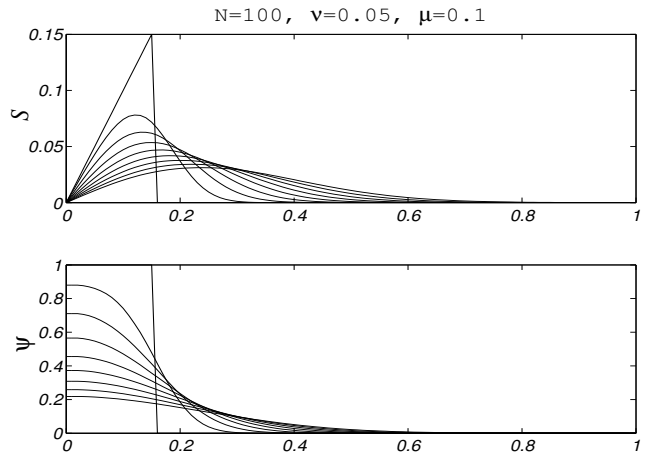

Figure 5.6: Flux-limited scheme using "superbee" limiter, $\lambda = 0.02$.

0.5pt0pt

Chapter 6

Conclusion

In this report, a model for radial squeeze flow of a homogeneous material between two approaching plates has been examined. Simplifying assumptions of uniform radial velocity and slip at the walls were used. Analytical solution of the resulting model was briefly discussed. To provide a background for the numerical solution of the radial model, numerical methods for the solution of conservation laws were investigated, focussing in particular on the technique of flux-limiting. This method is useful for preventing the generation of spurious oscillations in the solution, by imposing restrictions which cause the total variation of the solution to decrease over time. Having discussed numerical methods in general terms, the application of these methods to the radial flow model was described, taking into consideration variations due to the radial formulation. A flux-limited scheme for the radial flow model was formulated and issues arising from its implementation were considered. The numerical results obtained showed that the flux-limited scheme successfully removed oscillations arising in the second order Lax-Wendroff scheme.

Some possibilities for future research are

- an investigation of the ranges of the parameters ν and λ for which the flux-limited scheme gives valid solutions,
- more work on stability and convergence of the flux-limiter solution,
- an investigation of asymptotic expansions of the analytical solution for large or small values of the parameter λ,
- incorporation of more complicated rheological properties into the model,

- extension of the model to the situation of non-uniform flow, where it may be possible to use ideas from the analysis of Taylor dispersion,
- careful investigation of the correct outflow boundary condition for the model.

0.5pt0pt

Bibliography

[1] M. Abramowitz & I.A. Stegun (eds.), *Handbook of Mathematical Functions*, Wiley (1972).

[2] J. Bear, *Dynamics of Fluids in Porous Media*, Dover (1988).

[3] S.W. Churchill, *Viscous Flows, The Practical Use of Theory*, Butterworths (1988).

[4] S.F. Davies, *Shock capturing*, in Numerical Methods for Partial Differential Equations, S.I. Hariharan & T.H. Moulden, eds., Longman (1986).

[5] S.F. Davies, *A simplified TVD finite difference scheme via artificial viscosity*, SIAM J. Sci. Stat. Comput., 8(1) (1987), 1-15.

[6] A. Harten, *High resolution schemes for hyperbolic conservation laws*, J. Comp. Phys., 49 (1983), 357-393.

[7] C. Hirsch, *Numerical Computation of Internal and External Flows, v.2*, Wiley (1990).

[8] P.D. Lax, *Systems of Conservation Laws and the Mathematical Theory of Shock Waves*, SIAM (1973).

[9] R.J. LeVeque, *Numerical Methods for Conservation Laws*, Birkhäuser Verlag (1992).

[10] K.W. Morton, *Numerical Solution of Convection-Diffusion Problems*, Applied Mathematics and Mathematical Computation 12, Chapman & Hall (1996).

[11] K.W. Morton & D.F. Mayers *Numerical Solution of Partial Differential Equations - an introduction*, Cambridge (1994).

[12] J.D. Sherwood, *Liquid-solid relative motion during squeeze flow of pastes*, J. Non-Newtonian Fluid Mech., (2002).

[13] P.K. Sweby, *High resolution methods using flux limiters for hyperbolic conservation laws*, SIAM J. Num. Anal., 21 (1984), 995-1011.

Appendix A

Source code

```
function S = RoeFL(N,rShock,nu,lambda,Tfinal)
% ROEFL    Implement Roe flux limited scheme for radial flow model
%    N number of mesh points
%    rShock point where initial jump occurs
%    nu = dt/h
%    lambda = D/(U*R^2) problem dependent parameter
%    Tfinal final time for calculations

h = 1/N;                                          % Grid size
mu = lambda*nu/h;                                 % Calculate diffusion coefficient

TimeSteps = Tfinal/nu;                            % Determine number of iterations
plotEvery = TimeSteps/8;                          % and how often to plot

r = linspace(0,1,N+1);                            % Set up spatial domain
psi = (1:N+1)/N <= rShock;                        %   and initial condition
S = (r.*psi);

figure
subplot(211), plot(r,S), hold on,                 % Plot initial profiles
subplot(212), plot(r,psi), hold on

smallNumber = 1e-4;                               % Small and large numbers
bigNumber = 100;

for iter = 1:TimeSteps,
    f = r.*S;                                     % Exact flux at grid points
    DeltaS = S(2:N+1) - S(1:N);                   % Define differences
    Deltaf = f(2:N+1) - f(1:N);                   %   for S and f

    for i = 1:N
        if abs(DeltaS(i)) > smallNumber
            a(i) = Deltaf(i)/DeltaS(i);           % Evaluate a
        else
            a(i) = i*h;                           % df/ds(S_i)
        end
        Roeflux(i) = 0.5*(f(i) + f(i+1)) ...
- 0.5*abs(a(i))*DeltaS(i); % Evaluate Roe flux
    end

    for i = 1:N-1                                 % Evaluate flux ratios
```

```
                                            %   provided that it is safe to do so!
        if (abs(f(i) - Roeflux(i)) < smallNumber) ...
                & (abs(f(i+1) - Roeflux(i+1)) < smallNumber), thetaminus(i) = 0;
        elseif (abs(f(i) - Roeflux(i)) >= smallNumber) ...
                & (abs(f(i+1) - Roeflux(i+1)) < smallNumber), thetaminus(i) = bigNumber;
        else
            thetaminus(i) = (f(i) - Roeflux(i))./(f(i+1) - Roeflux(i+1));
        end
        if (abs(f(i+2) - Roeflux(i+1)) < smallNumber) ...
                & (abs(f(i+1) - Roeflux(i)) < smallNumber),   thetaplus(i) = 0;
        elseif (abs(f(i+2) - Roeflux(i+1)) >= smallNumber) ...
                & (abs(f(i+1) - Roeflux(i)) < smallNumber),   thetaplus(i) = bigNumber;
        else
            thetaplus(i) = (f(i+2) - Roeflux(i+1))./(f(i+1) - Roeflux(i));
        end
    end
    Phiminus = fluxLimiter(thetaminus, 'S');      % Evaluate flux limiters
    Phiplus =  fluxLimiter(thetaplus, 'S');       % 'M' = minmod, 'S' = superbee

    for i = 1:N-2                                 % Calculate second order flux
        F(i) = Roeflux(i+1) + 0.5*Phiplus(i)*(f(i) - Roeflux(i)) ...
            + 0.5*Phiminus(i)*(f(i+2) - Roeflux(i+1));
    end

    for i = 3:N-1
        rplus = (i+0.5)*h;
        rminus = (i - 0.5)*h;
        S(i) = S(i) - nu*(F(i-1) - F(i-2)) ...    % Perform update
            + mu*(rplus*(psi(i+1) - psi(i)) - rminus*(psi(i) - psi(i-1)));
    end

    S(2) = 0.5*(S(3) - S(1));                     % Approximate intermediate points
    S(N) = 0.5*(S(N+1) - S(N-1));

    psi(2:N+1) = S(2:N+1)./r(2:N+1);              % Update psi
    psi(1) = psi(2);

    if mod(iter, plotEvery) == 0                  % Plot
        subplot(211), plot(r,S), subplot(212), plot(r,psi)
    end
end
labelFig(N,nu,mu,'Flux-limited Roe scheme')

function Phi = fluxLimiter(theta,code)
switch code
case 'M'
    Phi = (theta>0).*min(theta,1);                      % Minmod limiter
case 'S'
    Phi = (theta>0).*max(min(2*theta,1), min(theta,2)); % Superbee limiter
end
```